Hindawi
Geofluids
Volume 2020, Article ID 8818293, 10 pages
https://doi.org/10.1155/2020/8818293

WILEY | Hindawi

Research Article

Experimental Measurement of the Transport Flow Path Aperture in Thermally Cracked Granite and the Relationship between Pore Structure and Permeability

Kazumasa Sueyoshi, Tadashi Yokoyama, and Ikuo Katayama

Graduate School of Advanced Science and Engineering, Hiroshima University, Kagamiyama, Higashi-Hiroshima, Hiroshima, Japan

Correspondence should be addressed to Kazumasa Sueyoshi; ksueyoshi@hiroshima-u.ac.jp

Received 8 May 2020; Revised 25 August 2020; Accepted 16 October 2020; Published 7 November 2020

Academic Editor: Nicoló Colombani

Fluid flow in rocks has a key role in many geological processes, such as in geothermal reservoirs and crustal deformation. Permeability is known to be dependent on porosity and flow path aperture, but direct quantification of pore structures is more difficult than direct estimation of permeability. The gas breakthrough method can be used to determine the radius of transport pores by using the gas pressure at which gas breaks through a water-saturated sample (ΔP_{break}). In this study, we applied the gas breakthrough method under confining pressure to damaged granite, in order to evaluate the relationship between permeability and pore characteristics (i.e., porosity and transport flow path aperture) at pressures up to 30 MPa. The transport flow path aperture, permeability, and porosity of thermally cracked granite decrease with increasing confining pressure. We quantified the relationship between permeability and pore characteristics, which provides a better estimation of permeability by taking into account the fraction of hydraulically connected cracks.

1. Introduction

Fluid flow in rocks has a key role in various geological processes, including crustal deformation [1, 2] and fluid-induced seismicity [3, 4]. Laboratory experiments on rock samples have yielded a wide range of permeabilities (10^{-12} to 10^{-23} m^2), controlled by lithology, porosity, and pore geometry (Gueguen and Palciauskas, 1994). Under differential stress, brittle deformation can rapidly change permeability and affect fluid flow processes due to dilatancy related to microcrack nucleation and growth [5, 6]. In contrast, an increase in hydrostatic pressure reduces permeability through the progressive closure of pores within a rock [7, 8]. Permeability is known to be sensitive to crack porosity and aperture, and a relationship between pore structure and permeability has been proposed based on the poroelastic medium theory [9–11].

The critical pore throat radius of a rock can be experimentally determined with the gas breakthrough method [12–15]. In this method, the gas pressure injected into one end of a water-saturated sample is increased. When the pressure overcomes the resistance due to the surface tension of water, the pore throat radius r is obtained from the gas breakthrough pressure ($\Delta\Delta P_{\text{break}}$) by the following equation of capillarity:

$$\Delta P_{\text{break}} = 2\gamma \cos\theta / r, \tag{1}$$

where γ is the surface tension of the gas–water interface and θ is the contact angle. This method has been applied to various materials including vesicular volcanic rocks, sandstones, and mudstones in order to determine sealing integrity or to evaluate the permeability-pore structure relationship but has not been applied to crystalline rocks for evaluating the effect of thermal cracking. In this study, the gas breakthrough method under confining pressure was used to determine the relationship between permeability, porosity, and flow path aperture under hydrostatic conditions in thermally cracked Aji granite.

2. Sample Description

For our experiments, we used samples of fine-grained granite from Aji, Japan. The average grain size of this granite is 0.3 mm, and it comprises 30 vol.% quartz, 37 vol.% plagioclase, 24 vol.% K-feldspar, and 8 vol.% biotite [16]. The samples have a bulk density of 2.66 g/cm^3 and an apparent initial porosity of 0.62% [17]. Based on elastic wave velocity measurements, textures within the Aji granite are near isotropic [18]. In our experiments, each sample was cut into a cylinder with a diameter of 20 mm and length of 20 mm (uncertainty of less than ±0.05 mm).

The Aji granite samples were heat-treated at room pressure up to 400°C, 600°C, and 800°C at a heating rate of 5°C/min. The samples were kept in an oven at each temperature for 2 h, after which the oven was turned off and the samples left to slowly cool overnight. As such, cracks were generated by thermal stressing due to the different thermal expansions of adjacent grains and from the α- to β-quartz transition at temperatures of >550°C [19]. Back-scattered electron images show that intergranular cracks form above 550°C; intragranular cracks were also observed (Figure 1).

3. Experimental Apparatus and Methods

For this study, permeability, flow path aperture, and porosity measurements were conducted under hydrostatic pressure at room temperature using an intravessel deformation and fluid flow apparatus (Figure 2) at Hiroshima University, Hiroshima, Japan [20]. The cylindrical samples were enclosed in polyolefin tubes to prevent interaction with the confining oil. Experimental methods for determination of (i) permeability and porosity and (ii) transport flow path aperture (gas breakthrough method) are presented in the following sections.

3.1. Permeability and Porosity Measurements. Permeability was measured with the flow method using water as a pore fluid, in which a constant upstream pore pressure was maintained (P_p = 0.5 – 3.0 MPa). The steady-state fluid flow driven by the pore pressure gradient across the sample was monitored using a syringe pump every 10 s. Permeability (k) was determined from the measured flow rate as follows:

$$k = \frac{\mu}{A}\frac{L}{P_1 - P_2}\bar{Q}, \tag{2}$$

where μ is the viscosity of the pore fluid, P_1 is the upstream pore pressure, P_2 is the downstream pore pressure (atmospheric pressure), A and L are the cross-sectional area and length of the sample, respectively, and $\bar{Q}$ is the mean flow rate measured through the volume change of the syringe pump. The error of the fluid volume measurement is $<16.63 \times 10^{-9}$ L in each time step.

We determined the porosity of granite thermally cracked at 400°C, 600°C, and 800°C with a gas porosimeter using nitrogen gas as a pore fluid [20]. The samples were first set in a pycnometer, and the grain volume was measured at atmospheric pressure using the gas expansion method based on Boyle's law (Table 1). We then placed the sample in the pressure vessel and measured the pore volume under confining pressure (Pc = 5 – 30 MPa) using a gas porosimeter attached to the apparatus. The porosity error is ca. ±0.01%.

3.2. Transport Flow Path Aperture Measurements (Gas Breakthrough Method). The gas breakthrough method is used to determine the pore throat radius (e.g., [15]). When gas is injected at the bottom of the water-saturated sample, the gas pressure pushes the gas–water interface whereas the surface tension acts as a resistance to the gas pressure. The pressure difference between the gas–water interface and air is correlated to flow path aperture w (minor radius) by the following equation for capillarity and assuming that the flow path cross-section is an ellipse:

$$w = \frac{\gamma I \cos\theta}{\pi a \Delta P}, \tag{3}$$

where I is the circumference of the ellipse and can be expressed as follows:

$$I = 4a\int_0^{\pi/2}\sqrt{1 - A^2\cos^2\psi}\,d\psi, \tag{4}$$

where γ (N/m) is the surface tension, θ is the contact angle between the rock and water, ΔP (Pa) is the differential pressure at the gas–water interface, a is the long-axis length of the ellipse (major radius), and A (= w/a) is the aspect ratio of the flow path cross-section. Gas flows through the sample when the gas pressure overcomes the surface tension at the position of the smallest aperture in the most preferential flow path. The characteristic flow path aperture can be determined from the pressure difference at which the first gas flow occurs (breakthrough pressure ΔP_{break}). During the experiments, the samples were first saturated with water (during the permeability measurement phase), as shown in Figure 2(b), and then, nitrogen gas was injected from the bottom of the samples at a constant flow rate of 2.5 mL/min using a syringe pump. The upstream part of the sample was connected to a water tank. When the first bubble appeared in the water tank, we recorded the gas pressure as ΔP_{break} (Figure 2(c)). The contact angle θ between the rock and water was assumed to be 52°, which has been measured in the water–air system for Westerly granite [21]. We used a nitrogen–water interfacial tension of 0.075–0.072 N/m [22], depending on the measured room temperature (10–25°C). The error on the flow path aperture is 0.000072–0.26 μm for our samples with apertures of 0.13–8.0%, based on the uncertainty of the gas pressure measurement by the syringe pump.

4. Experimental Results

The experimental results for transport flow path aperture, permeability, and porosity are listed in Table 2. Figure 3(a) shows the variation of ΔP_{break} with confining pressure, where ΔP_{break} tends to increase systematically with confining pressure. Figure 3(b) shows the flow path aperture calculated from ΔP_{break} as a function of confining pressure. The flow path aperture decreases with increasing confining pressure

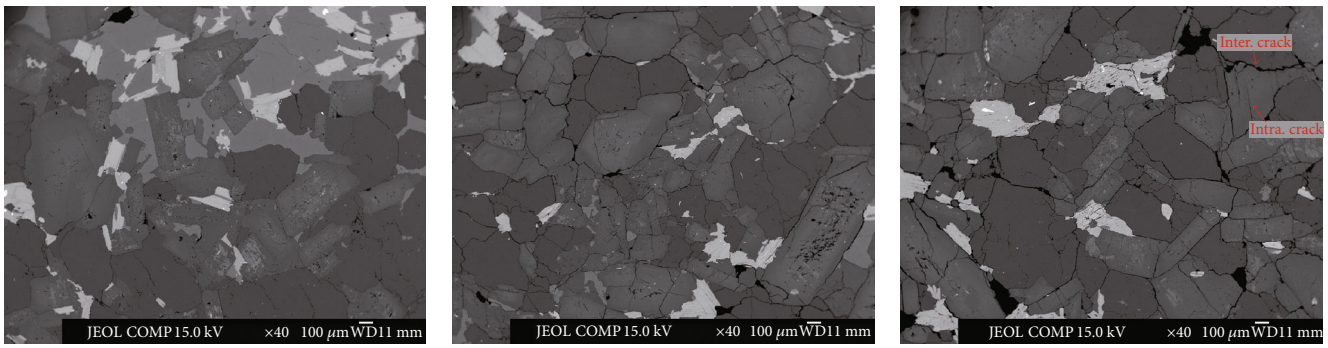

(a) (b) (c)

FIGURE 1: Back-scattered electron images of Aji granite heat-treated at (a) 400°C, (b) 600°C, and (c) 800°C. Inter. crack: intergranular crack; Intra. crack: intragranular crack.

for all samples, although the flow path apertures are considerably smaller for the sample treated at 400°C. This suggests that thermal damage due to the α- to β-quartz transition results in significant crack opening.

Figure 4 shows that the permeability decreased with increasing confining pressure. During hydrostatic loading, the permeability decreased by an order of magnitude for all samples. The samples heated at 400°C, 600°C, and 800°C show a reduction in permeability with increasing effective pressure, ranging from 1.61×10^{-18}, 8.50×10^{-17}, and 2.72×10^{-16} m^2 at 5 MPa to 1.70×10^{-19}, 5.16×10^{-18}, and 1.24×10^{-17} m^2 at 30 MPa, respectively. Porosity measurements also showed a systematic change with applied confining pressure (Figure 5). Porosity shows a large variation at 5 MPa (1.4%–2.6%) that decreases with confining pressure (1.0%–1.5% at 30 MPa).

5. Discussion

5.1. Analysis Based on Percolation Theory. Percolation theory predicts a power law relationship between porosity and permeability in the form of the following equation (e.g., [9]):

$$k = C(\phi - \phi_{cr})^e, \tag{5}$$

where C (m^2) is a constant term that determines the magnitude of the permeability, e is a critical exponent, and ϕ_{cr} is the porosity at the percolation threshold, which is the minimum porosity at which fluid flow occurs across the sample ($k = 0$ for $\phi < \phi_{cr}$ and $k > 0$ for $\phi \geq \phi_{cr}$). ϕ_{cr} and e are important parameters in percolation theory and depend on the geometry of the pore structure assumed in the model. For our samples, the relationship between porosity ϕ and permeability k can be approximated by the equation $k = 1.76 \times 10^{-11}(\phi - 0.00855)^{2.77}$, based on percolation theory (Figure 6). Figure 7 shows a plot of permeability versus porosity, including published data for sandstone, hot-pressed materials, and granite [23–27]. The obtained data are distributed within the previously reported regression lines for sandstone and granite.

For a medium in which permeation occurs through interconnected and randomly distributed thin cracks, the following model has been used [28, 29]:

$$k \simeq \frac{16\alpha\xi^2\left(1-\xi^2\right)\phi c^2}{9\left[2\sqrt{1-\xi^2}+\xi^2\log\left(\left(2-\xi^2+2\sqrt{1-\xi^2}\right)/\xi^2\right)\right]^2}, \tag{6}$$

where c is the crack radius and ξ is the aspect ratio ($= w/c$), which is assumed to be constant at $\xi = 0.001$. The constant α is dimensionless and depends on the tortuosity of the crack network τ and shape factor b as follows [30, 31]: $\alpha = 1/(b^2\tau^2)$. Tortuosity τ was calculated by inserting the measured values of k and w^2 ($= \xi^2 c^2$) into Eq. (6), to evaluate the relevance of τ to k. Tortuosity decreased with decreasing permeability, ranging from 17 to 3 (Figure 8). Pore connectivity is related to the reciprocal of the tortuosity squared [32]. Thus, the tortuosity reduction corresponds to increasing crack network connectivity. Our results indicate that the connectivity increases with decreasing porosity due to the closure of cracks. Details of the calculation are given in the next section.

5.2. Relationships between Permeability, Porosity, and Flow Path Aperture. Several models have been used to predict the permeability of rocks from microstructural parameters [11, 32, 33]. By assuming that the cracks are thin disks of variable length, the permeability during brittle deformation can be estimated using crack parameters as follows:

$$k \propto \phi w^2, \tag{7}$$

where ϕ is the crack porosity, calculated as follows:

$$\phi = 2\pi\frac{c^2 w}{l^3}, \tag{8}$$

where $2c$ is the crack length, w is the crack aperture, and l is the crack spacing [32]. Equation (7) indicates that the permeability is sensitive to the crack aperture. To examine the applicability of Eq. (7) to our results, we investigated the relationship between permeability k and ϕw^2 (Figure 9). Although Eq. (7) indicates that k and ϕw^2 have a linear

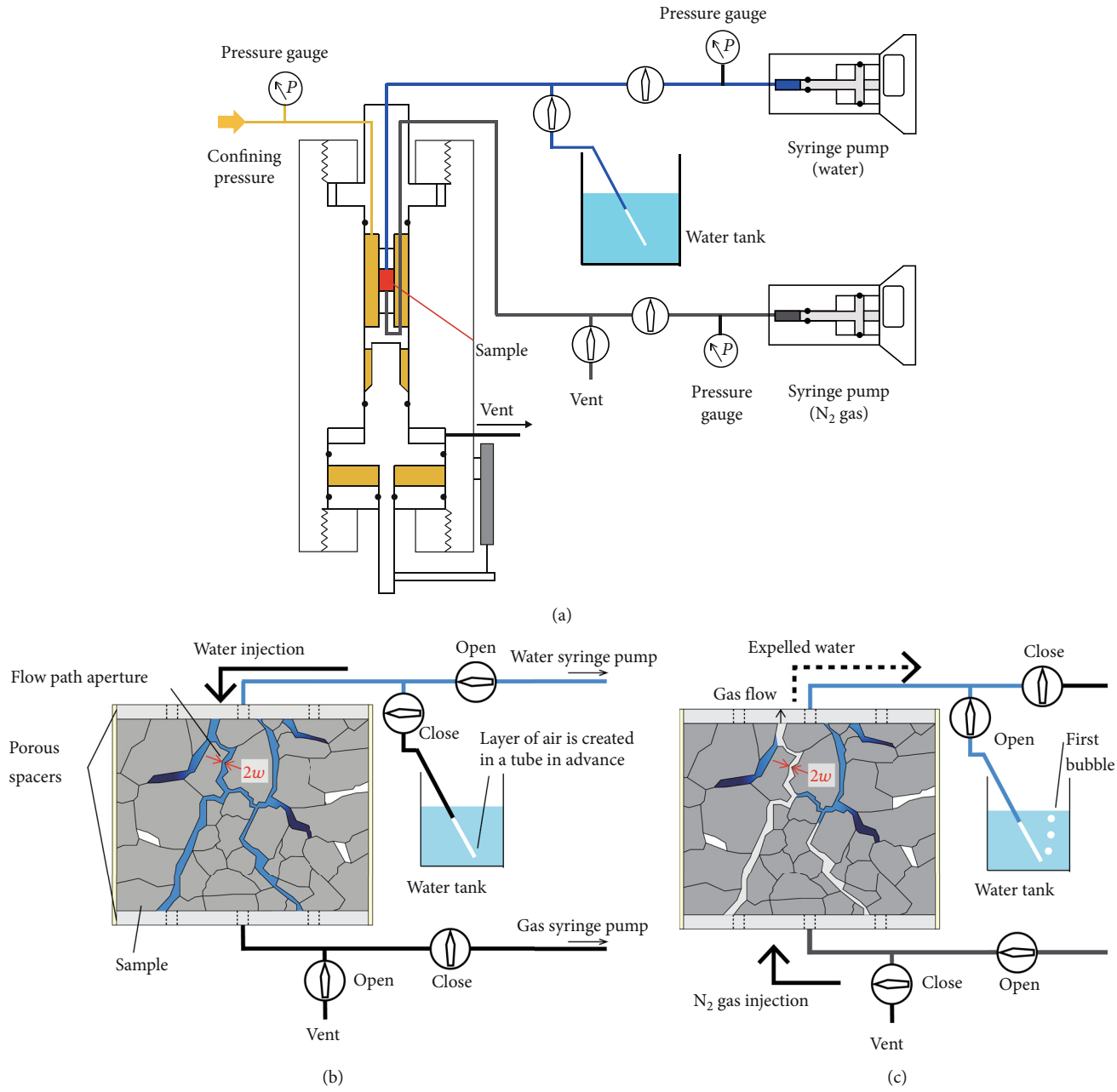

FIGURE 2: (a) Experimental design of the gas breakthrough method using the intravessel deformation fluid flow apparatus. Simplified illustrations of the (b) permeability measurement phase and (c) gas breakthrough experiment.

TABLE 1: Sample description.

Treated temperature ˚C	Initial porosity %	Density g/cm^3
400	2.86	2.64
600	3.38	2.60
800	4.51	2.57

relationship, the log–log plot of our data shows that the data are well approximated by $k = 8.64 \times 10^{-9}(\phi w^2)^{0.615}$ and not distributed on a line with a slope of one. This suggests that k is not a simple linear function of ϕw^2. Nishiyama and Yokoyama [14] also showed that k of many granular media is correlated with a power function of ϕr_{cr}^2 ($k = 8.5(\phi r_{cr}^2)^{1.3}$) (Figure 10), where r_{cr} (= w) is the critical pore radius. The nonlinear relationship between k and ϕw^2 suggests that another factor needs to be considered in the permeability evolution at elevated hydrostatic pressure.

Gueguen and Dienes [32] showed that permeability k can be expressed as follows:

$$k = \frac{2}{15} f \phi w^2, \tag{9}$$

Table 2: Summary of experimental results.

Treated temperature ˚C	Pc MPa	ΔP_{break} MPa	w μm	Pp MPa	k m^2	Porosity %
	5	0.850-0.885	0.103-0.107	0.5	1.22×10^{-18}-1.61×10^{-18}	1.38
	7.5	1.21-1.59	0.0573-0.0754	0.75	8.06×10^{-19}-9.48×10^{-19}	1.32
	10			1	6.86×10^{-19}	1.24
400	15			1.5	4.21×10^{-19}	1.13
	20			2	2.85×10^{-19}	1.07
	25			2.5	2.19×10^{-19}	1.02
	30			3	1.70×10^{-19}	0.990
	5	0.039-0.048	1.87-2.30	0.5	8.11×10^{-17}-8.50×10^{-17}	1.83
	7.5	0.056-0.062	1.45-1.60	0.75	4.47×10^{-17}-5.33×10^{-17}	1.66
	10	0.074-0.078	1.15-1.21	1	3.11×10^{-17}-3.26×10^{-17}	1.50
600	15	0.113-0.124	0.723-0.794	1.5	1.69×10^{-17}-1.82×10^{-17}	1.33
	20	0.154-0.188	0.476-0.581	2	9.64×10^{-18}-9.96×10^{-18}	1.22
	25	0.238-0.275	0.326-0.376	2.5	6.86×10^{-18}-7.20×10^{-18}	1.17
	30	0.351-0.362	0.247-0.255	3	5.16×10^{-18}-5.34×10^{-18}	1.11
	5			0.5	2.50×10^{-16}-2.72×10^{-16}	2.66
	7.5	0.027-0.028	3.18-3.30	0.75	1.39×10^{-16}-1.43×10^{-16}	2.44
	10	0.041	2.18	1	9.96×10^{-17}-1.00×10^{-16}	2.21
800	15	0.063-0.065	1.38-1.42	1.5	4.80×10^{-17}-5.02×10^{-17}	1.91
	20	0.081-0.096	0.936-1.08	2	2.72×10^{-17}-2.79×10^{-17}	1.72
	25	0.126-0.140	0.642-0.713	2.5	1.89×10^{-17}-1.95×10^{-17}	1.58
	30	0.181-0.192	0.468-0.496	3	1.24×10^{-17}-1.26×10^{-17}	1.50

Pc = confining pressure; Pp = pore pressure from the permeability measurement; k = permeability; ΔP_{break} = gas breakthrough pressure; w = flow path aperture.

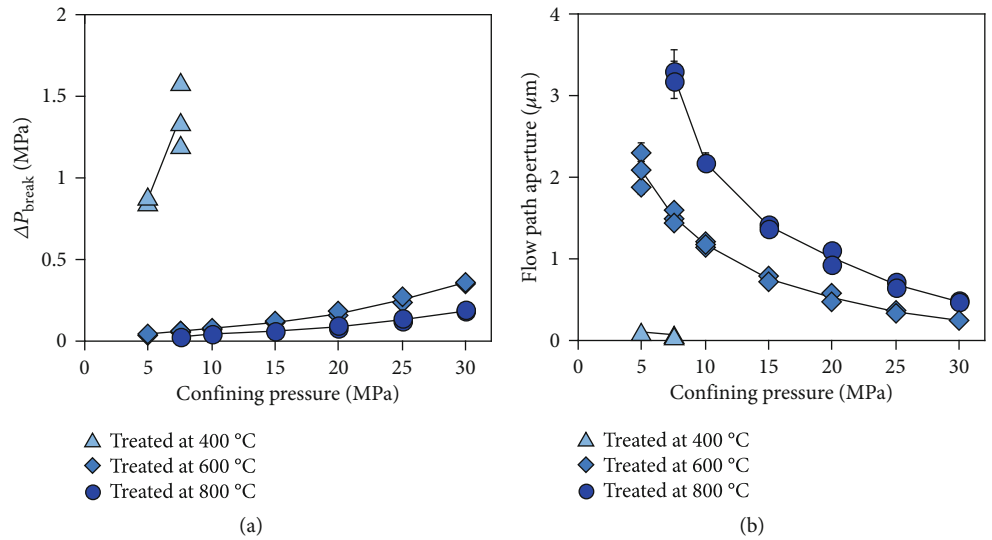

Figure 3: (a) Evolution of ΔP_{break} and (b) flow path aperture as a function of confining pressure. The light blue triangle, blue square, and dark blue circle represent experiments conducted using samples that were thermally damaged at 400˚C, 600˚C, and 800˚C, respectively.

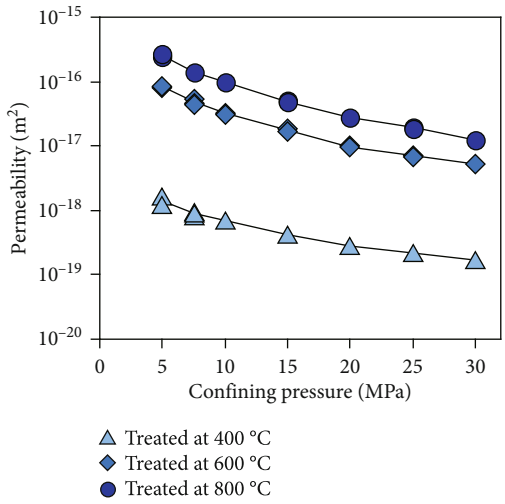

Figure 4: Evolution of permeability as a function of confining pressure.

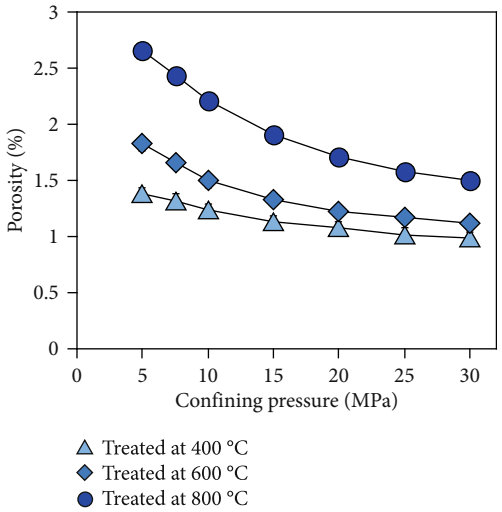

Figure 5: Plot of porosity versus confining pressure.

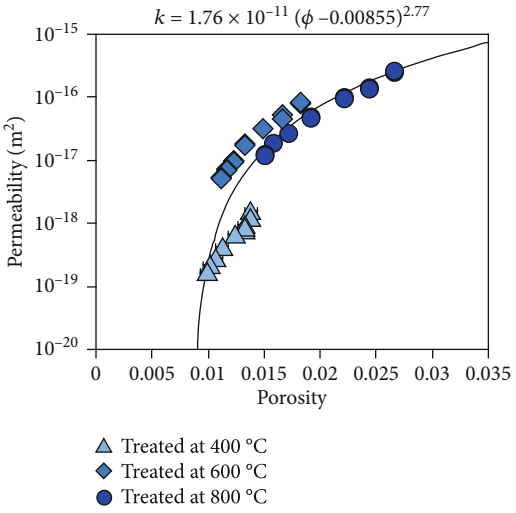

Figure 6: Plot of permeability versus porosity.

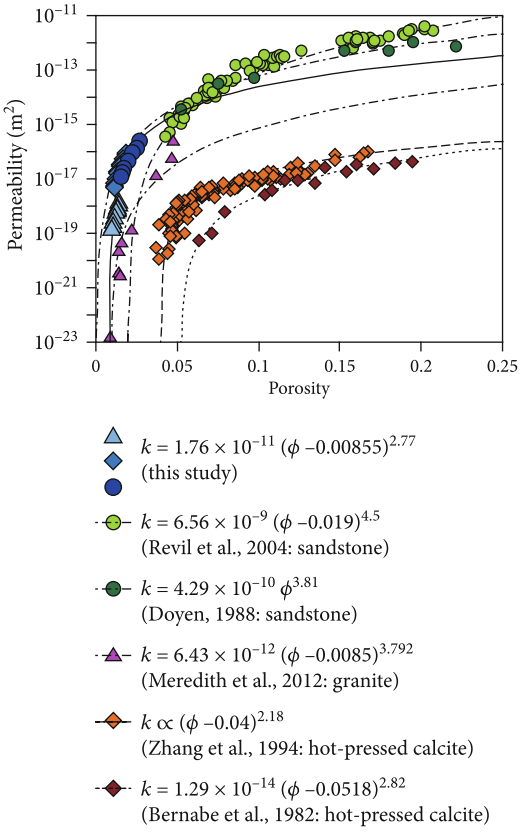

Figure 7: Comparison of our experimental data on permeability-porosity relationship with those for various rock types, including sandstone, hot-pressed calcite, and granite, published in previous experimental studies.

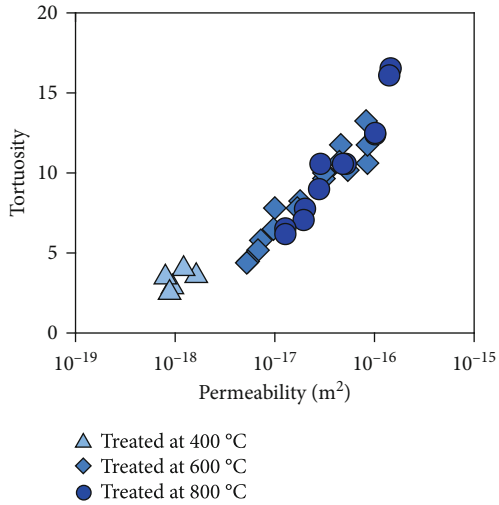

Figure 8: Evolution of tortuosity as a function of permeability.

where f is the fraction of cracks that contribute to the flow, which is zero when the probability of crack intersection is below the percolation threshold [34]. Note that f differs from the crack network connectivity described in the previous section. If k decreases, the network connectivity invariably decreases, but f can increase if ϕw^2 decreases more than k.

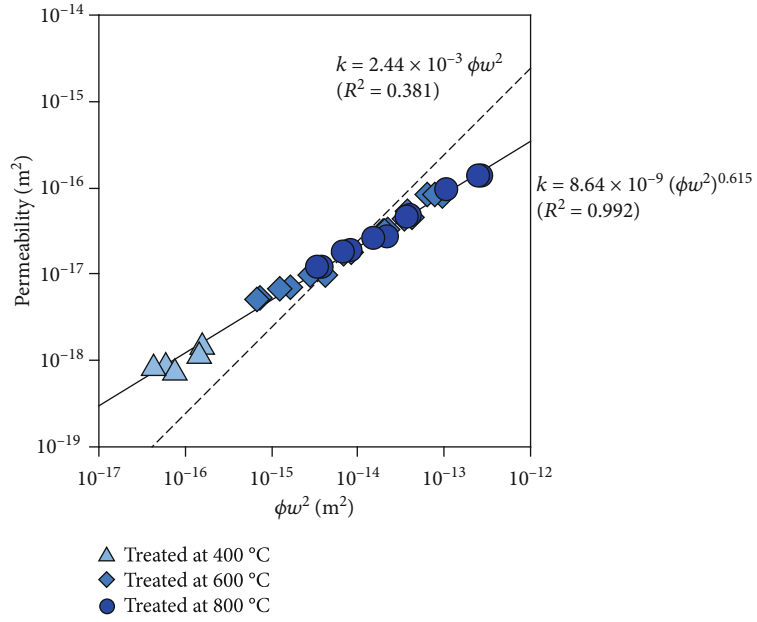

Figure 9: Plot of k versus ϕw^2. The fitted straight line is based on a constant coefficient for ϕw^2 and the relationship between k and ϕw^2 described in the main text. The dashed line has a slope of one on a log–log plot.

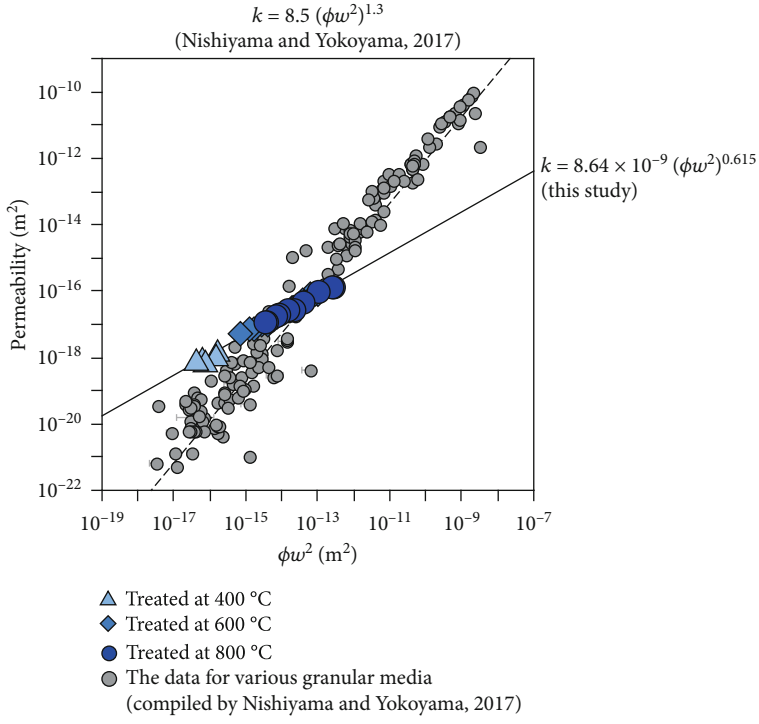

Figure 10: Comparison of our experimental data on permeability-ϕw^2 relationship with those of previous experimental studies compiled by Nishiyama and Yokoyama [14].

f is the ratio of interconnected cracks to the total cracks and can be expressed as follows:

$$f = 1 - 4Q^3 + 3Q^4, \tag{10}$$

where Q is the probability that a path from one site passing through an adjacent site will be interrupted (Gueguen and Palciauskas, 1994). This suggests that the connectivity factor f represents flow paths that belong to the infinite cluster and propagate in various directions. However, we determined the

permeability from the flow rate in the axial direction of the sample (Figure 11). Therefore, the permeability obtained in this study needs to be expressed by a connectivity factor that is different from f.

In this study, F is defined as a new factor that represents the fraction of cracks that contribute to flow in the axial direction of the sample. We can modify Eq. (9) using F instead of f as follows:

$$k = \frac{2}{15} F\phi w^2. \tag{11}$$

F was calculated by inserting the measured values of k and ϕw^2 into Eq. (11), in order to evaluate the relevance of F to k. A plot of F versus k shows that F increases with decreasing k (Figure 12). The relationship between F and k is approximated by the following equation:

$$F = 9.31 \times 10^{-13} k^{-0.614}. \tag{12}$$

This indicates that although the connectivity in the flow path network is significantly reduced with decreasing permeability, the fraction of cracks that contribute to flow in the axial direction of the sample increases; consequently, fluid flow is mostly dominated by a specific path in a relatively impermeable medium (Figure 13). The existence of preferential flow paths has been proposed based on numerical simulations of two-dimensional heterogeneous systems, which have been used as an analog for pore geometry in porous rocks [35, 36]. Our experimental results for thermally cracked granite suggest that permeability is dependent not only on porosity and flow path aperture but also on the fraction of cracks that contribute to flow.

We investigated the relationship between permeability and pore characteristics by taking into account the fraction of hydraulically connected cracks that contribute to flow in the axial direction under confining pressure. The variable F appears to be required for the case where fluid flow occurs in a specific direction in the subsurface (e.g., the production of geothermal energy by fluid flow in the direction between the inlet and outlet wells).

6. Conclusions

We have presented experimental data for the permeability, porosity, and flow path aperture of thermally cracked granite under hydrostatic conditions. Using the gas breakthrough method, we measured the crack aperture of samples subjected to elevated pressure. In all experiments, the confining pressure increased as permeability decreased, due to the closure of cracks. Based on the relationships between permeability, porosity, and flow path aperture, permeability is inferred to be controlled mainly by variations in the crack aperture as follows: $k = 8.64 \times 10^{-9} (\phi w^2)^{0.615}$. A comparison of the obtained equation with the permeability model [32] indicates that fluid flow is more concentrated on a specific path with decreasing permeability. To obtain a more detailed permeability model, quantitative analysis of the effects of geometric factors, such as the crack network and aperture, at hydrostatic pressures is required.

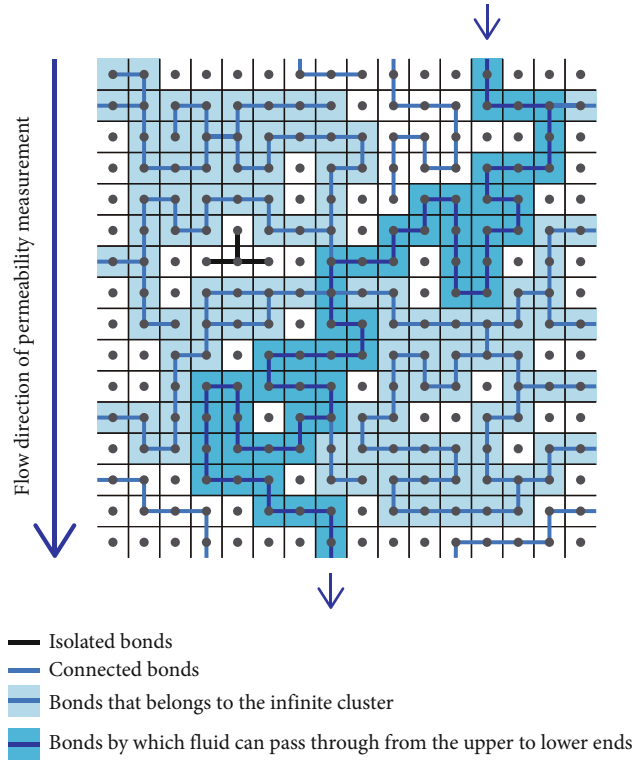

Figure 11: Schematic illustration of paths that contribute to the flow described in previous studies (Gueguen and Palciauskas, 1994) and this study due to bond percolation. The presence of a bond between spheres reflects the ability of fluid to flow. The light blue bonds are related to the factor f, and the dark blue bonds are related to the factor F.

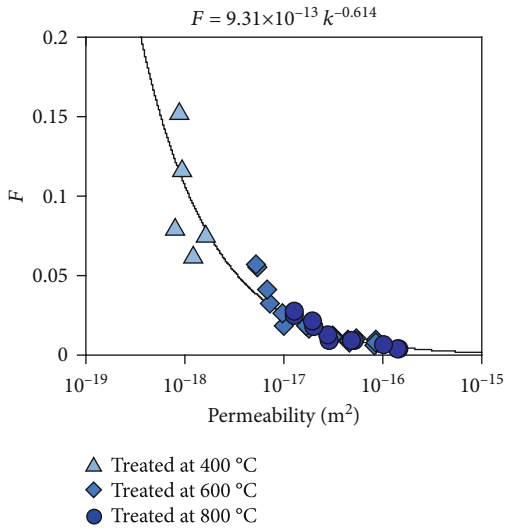

Figure 12: Plot of F versus k.

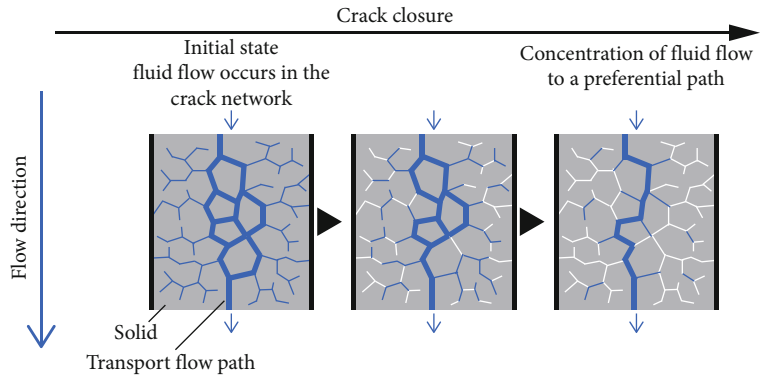

Figure 13: Schematic illustration of variations in flow path geometry. Blue bold line: flow paths that are open to both the upper and lower ends of the sample (transport flow path); blue thin line: flow paths that are connected to the transport flow path but come to a dead-end or are isolated.

Data Availability

The experimental data used to support the findings of this study are included within the article.

Conflicts of Interest

The authors declare that there is no conflict of interest regarding the publication of this paper.

Acknowledgments

We thank Y. Shibata for undertaking the back-scattered electron image analysis. We are grateful to N. Nishiyama for discussions regarding this research. We thank Ian Jackson and Joel Sarout for their thoughtful and constructive comments. This study was partially supported by the Japan Society for the Promotion of Science (Grants 18H01321 and 18H03733).

References

[1] J. D. Byerlee, "The fracture strength and frictional strength of Weber sandstone," *International Journal of Rock Mechanics and Mining Sciences & Geomechanics Abstracts*, vol. 12, no. 1, pp. 1–4, 1975.

[2] R. H. Sibson, "Structural permeability of fluid-driven fault-fracture meshes," *Journal of Structural Geology*, vol. 18, no. 8, pp. 1031–1042, 1996.

[3] P. Talwani and S. Acree, "Pore pressure diffusion and the mechanism of reservoir-induced seismicity," *Pure and Applied Geophysics PAGEOPH*, vol. 122, no. 6, pp. 947–965, 1984.

[4] H. Velcin, J. Dautriat, J. Sarout, L. Esteban, and B. Godel, "Experimental reactivation of shear-fractured Berea and Boise sandstones by brine or liquid CO_2 injection at depth," *Journal of Geophysical Research: Solid Earth*, vol. 125, no. 2, pp. 1–25, 2020.

[5] T. M. Mitchell and D. R. Faulkner, "Experimental measurements of permeability evolution during triaxial compression of initially intact crystalline rocks and implications for fluid flow in fault zones," *Journal of Geophysical Research: Solid Earth*, vol. 113, no. B11, pp. 1–16, 2008.

[6] M. D. Zoback and J. D. Byerlee, "The effect of microcrack dilatancy on the permeability of westerly granite," *Journal of Geophysical Research*, vol. 80, no. 5, pp. 752–755, 1975.

[7] W. F. Brace, J. B. Walsh, and W. T. Frangos, "Permeability of granite under high pressure," *Journal of Geophysical Research*, vol. 73, no. 6, pp. 2225–2236, 1968.

[8] J. Fortin, S. Stanchits, S. Vinciguerra, and Y. Guéguen, "Influence of thermal and mechanical cracks on permeability and elastic wave velocities in a basalt from Mt. Etna volcano subjected to elevated pressure," *Tectonophysics*, vol. 503, no. 1–2, pp. 60–74, 2011.

[9] M. Sahini and M. Sahimi, *Applications Of Percolation Theory*, CRC Press, London, 1994.

[10] G. Simpson, Y. Guéguen, and F. Schneider, "Permeability enhancement due to microcrack dilatancy in the damage regime," *Journal of Geophysical Research: Solid Earth*, vol. 106, no. B3, pp. 3999–4016, 2001.

[11] J. B. Walsh and W. F. Brace, "The effect of pressure on porosity and the transport properties of rock," *Journal of Geophysical Research*, vol. 89, no. B11, pp. 9425–9431, 1984.

[12] T. Fujii, S. I. Uehara, and M. Sorai, "Impact of effective pressure on threshold pressure of Kazusa group mudstones for CO_2 geological sequestration," *Materials Transactions*, vol. 56, no. 4, pp. 519–528, 2015.

[13] A. Hildenbrand, S. Schlömer, B. M. Krooss, and R. Littke, "Gas breakthrough experiments on pelitic rocks: comparative study with N2, CO2 and CH4," *Geofluids*, vol. 4, no. 1, p. 80, 2004.

[14] N. Nishiyama and T. Yokoyama, "Permeability of porous media: role of the critical pore size," *Journal of Geophysical Research: Solid Earth*, vol. 122, no. 9, pp. 6955–6971, 2017.

[15] T. Yokoyama and S. Takeuchi, "Porosimetry of vesicular volcanic products by a water-expulsion method and the relationship of pore characteristics to permeability," *Journal of Geophysical Research*, vol. 114, no. B2, article B02201, 2009.

[16] Y. Kudo, O. Sano, N. Murashige, Y. Mizuta, and K. Nakagawa, "Stress-induced crack path in Aji granite under tensile stress," *Pure and Applied Geophysics PAGEOPH*, vol. 138, no. 4, pp. 641–656, 1992.

[17] H. Yukutake, "Fracturing process of granite inferred from measurements of spatial and temporal variations in velocity during triaxial deformations," *Journal of Geophysical Research*, vol. 94, no. B11, pp. 15639–15651, 1989.

[18] T. Watanabe and A. Higuchi, "Simultaneous measurements of elastic wave velocities and electrical conductivity in a brine-saturated granitic rock under confining pressures and their implication for interpretation of geophysical observations," *Progress in Earth and Planetary Science*, vol. 2, no. 1, 2015.

[19] P. W. J. Glover, P. Baud, M. Darot et al., "*A*/*B* phase transition in quartz monitored using acoustic emissions," *Geophysical Journal International*, vol. 120, no. 3, pp. 775–782, 1995.

[20] K. Okazaki, H. Noda, S. Uehara, and T. Shimamoto, "Permeability, porosity and pore geometry evolution during compaction of Neogene sedimentary rocks," *Journal of Structural Geology*, vol. 62, pp. 1–12, 2014.

[21] C. H. Gates, E. Perfect, B. S. Lokitz, J. W. Brabazon, L. D. McKay, and J. S. Tyner, "Transient analysis of advancing contact angle measurements on polished rock surfaces," *Advances in Water Resources*, vol. 119, pp. 142–149, 2018.

[22] The Chemical Society of Japan, *Chemical Handbook (Basic) partII*, Maruzen, 5th edition, 2004.

[23] Y. Bernabe, W. F. Brace, and B. Evans, "Permeability, porosity and pore geometry of hot-pressed calcite," *Mechanics of Materials*, vol. 1, no. 3, pp. 173–183, 1982.

[24] P. M. Doyen, "Permeability, conductivity, and pore geometry of sandstone," *Journal of Geophysical Research*, vol. 93, no. B7, pp. 7729–7740, 1988.

[25] P. G. Meredith, I. G. Main, O. C. Clint, and L. Li, "On the threshold of flow in a tight natural rock," *Geophysical Research Letters*, vol. 39, no. 4, pp. 1–5, 2012.

[26] A. Revil, P. Kessouri, and C. Torres-Verdín, "Electrical conductivity, induced polarization, and permeability of the Fontainebleau sandstone," *Geophysics*, vol. 79, no. 5, pp. D301–D318, 2014.

[27] S. Zhang, M. S. Paterson, and S. F. Cox, "Porosity and permeability evolution during hot isostatic pressing of calcite aggregates," *Journal of Geophysical Research*, vol. 99, no. B8, pp. 15741–15760, 1994.

[28] J. Sarout, E. Cazes, C. Delle Piane, A. Arena, and L. Esteban, "Stress-dependent permeability and wave dispersion in tight cracked rocks: experimental validation of simple effective medium models," *Journal of Geophysical Research: Solid Earth*, vol. 122, no. 8, pp. 6180–6201, 2017.

[29] J. Sarout, "Impact of pore space topology on permeability, cut-off frequencies and validity of wave propagation theories," *Geophysical Journal International*, vol. 189, no. 1, pp. 481–492, 2012.

[30] Y. Bernabe, "Pore volume and transport properties changes during pressure cycling of several crystalline rocks," *Mechanics of Materials*, vol. 5, no. 3, pp. 235–249, 1986.

[31] M. S. Paterson, "The equivalent channel model for permeability and resistivity in fluid-saturated rock-a re-appraisal," *Mechanics of Materials*, vol. 2, no. 4, pp. 345–352, 1983.

[32] Y. Gueguen and J. Dienes, "Transport properties of rocks from statistics and percolation," *Mathematical Geology*, vol. 21, no. 1, pp. 1–13, 1989.

[33] A. Costa, "Permeability-porosity relationship: a reexamination of the Kozeny-Carman equation based on a fractal pore-space geometry assumption," *Geophysical Research Letters*, vol. 33, no. 2, pp. 1–5, 2006.

[34] M. Ravalee and Y. Guéguen, "Permeability models for heated saturated igneous rocks," *Journal of Geophysical Research*, vol. 99, no. B12, pp. 24251–24261, 1994.

[35] Y. Bernabe, "The transport properties of networks of cracks and pores," *Journal of Geophysical Research: Solid Earth*, vol. 100, no. B3, pp. 4231–4241, 1995.

[36] C. David, "Geometry of flow paths for fluid transport in rocks," *Journal of Geophysical Research*, vol. 98, no. B7, pp. 12267–12278, 1993.